Analysis of Surface Structure with Regard to Interfacial Delamination in Polyester Films with Incompatible Polymers

Katsuya Ito,[1] Chisato Nonomura,[1] Katsuhisa Yamashita,[1] Toshitake Suzuki,[1] Charoen Chinwanitcharoen,[2] Toshiro Yamada,[2] Hideaki Ishihara[3]

[1]*Toyobo Co., Ltd., Research Center, 1-1 Katata 2-chome, Otsu, Shiga 520-0292, Japan*
[2]*Kanazawa University, 40-20 Kodatsuno 2-chome, Kanazawa, Ishikawa 920-8667, Japan*
[3]*Kyoto Institute of Technology, Matsugasaki, Sakyo-ku, Kyoto 606-8585, Japan*

Received 7 March 2003; accepted 9 September 2003

ABSTRACT: Poly(ethylene terephthalate) (PET) films containing incompatible polymer particles were analyzed, with particular reference to the relationship between the PET particle interfacial tension and the microvoids, or the protrusion that were formed when the composite material was stretched at 90°C. A model was developed to simulate void formation and surface protrusion due to interfacial delamination between PET and three types of dispersed incompatible polymers, poly(4-methyl-1-pentene), polypropylene, and polystyrene. The numerical results, obtained with the finite element method, were compared with experimental data of the blends for both the internal and subsurface regions. The experimental measurements showed that the increase in the difference in the surface tension between PET and the added incompatible polymer was associated with the formation of larger voids. The protrusions were also generated in the stretching and delamination between PET and the incompatible polymers, but a decrease in the interfacial tension agreed with the formation of a larger protrusion. Modeling studies showed that increasing the interfacial tension between the two components in a blend causes a decrease in the critical stress for delamination. Interfacial tension values related qualitatively to the critical stress for void formation and protrusion calculated with the numerical analysis. A concavity was also necessary for understanding the surface structure of the films, along with protrusion.
 J Appl Polym Sci 92: 1243–1251, 2004

Key words: films; polyesters; surfaces; voids; interfaces

INTRODUCTION

Biaxially stretched polyester films made from poly(ethylene terephthalate) (PET) or poly(naphthalene terephthalate) have various applications[1,2] because of their advantages in dynamic properties, chemical properties, a heat property, an electrical property, and optical properties. When the surface state is controlled, these materials also have a variety of applications. Several kinds of coatings can be applied to give them adhesive, ink-receptive, and hydrophilic properties on the surface.[3–5] Sputter, plasma,[6,7] and corona processing[8] can also be applied to improve their adhesive properties. Many studies have also been done to control their surface geometry[2,9–11] because surface roughness (R_a) is also important for the total performance of a PET film.

An opaque PET film was also developed by the introduction of inorganic pigments or incompatible polymer particles into the PET matrix for cards, labels, and printing materials. Because the film containing the incompatible polymer particles had a lower density and a paper-like texture, it was called *synthetic paper* and was made from polyester. For this kind of synthetic paper, a surface modification was also performed to improve its printing properties, ability to be written on, and paper-like appearance.[12–15] This surface modification is usually carried out by the coating and introduction of inorganic pigment or incompatible polymer particles into the PET matrix.

Void-containing PET films made by the introduction of incompatible polymer particles have many interesting properties, including a lower density, compressibility, opacity, molding properties, and a paper-like texture. These interesting properties depend on the size and number of voids in the PET matrix. Voids are generated by interfacial delamination between PET and the incompatible polymer in the stretching process of the PET film, in which fine incompatible polymer particles disperse. In the process of void generation in the PET matrix, the surface protrusions are simultaneously formed, and these protrusions make the film surface rougher and more paper-like in appearance. To control these interesting bulk and surface properties of void-containing PET films, it is ex-

Correspondence to: T. Yamada (tyamada@t.kanazawa-u.ac.jp).

Journal of Applied Polymer Science, Vol. 92, 1243–1251 (2004)

TABLE I
Interfacial Energy Between PET and the Incompatible Polymer at 90°C

Material	γ_1 (mN/m)	γ_2 (mN/m)	γ_{12} (mN/m)
PET/TPX	40.1	21.1	10.8
PET/PP	40.1	25.5	9.43
PET/PS	40.1	35.7	0.59

tremely important to understand the void generation process by stretching. The interfacial delamination process and surface-protrusion-generation process are particularly interesting and important.

In a previous study, it was revealed that interfacial delamination (i.e., the void formation process) is strongly influenced by the interfacial tension between the PET matrix and the incompatible polymer particles, and the interfacial tension is a key factor in the determination of the void size.[16,17] In this study, we measured the R_a of void-containing PET films with various kinds of incompatible polymer particles (i.e., various kinds of interfacial tension) and compared them with results of a numerical analysis. We explain the studies in detail herein.

EXPERIMENTAL

Materials

PET with an intrinsic viscosity of 0.62 was used. Three kinds of polyolefine polymers, poly(4-methyl-1-pentene) (TPX; Mitsui Chemical, Tokyo, Japan), polypropylene (PP; Mitsui Noblen, Tokyo, Japan), and polystyrene (PS; Mitsui Toatsu Chemistry, Tokyo, Japan) were used as the incompatible polymers.

PET was blended with a certain amount of each incompatible polymer; the blends were molded into sheets by a twin-screw extruder (Ikegai Koki, model PCM30, Tokyo, Japan). The extruder temperature was 285°C. In each of blends, the ratio of PET to incompatible polymer was 93:7, 86:14, and 81:19 vol %. These three incompatible polymers were chosen because they had a large range of different values of surface tension. Table I shows the values of the surface tension for PET (γ_1) and the surface tension of the incompatible polymers, TPX, PP, and PS (γ_2). The interfacial energy for each pair of polymers (γ_{12}), calculated by Wu's equation,[19] is also shown in the Table I. The three types of unstretched sheets obtained were stretched in one direction at 90°C with a stretcher (Toyo Seiki, type 586, Tokyo, Japan) to a draw ratio of 3.0 [uniaxial tensile strain (ε) = 2.0]. The strain rate was 0.333 s^{-1}.

Measurements

The load-displacement curves for numerical analysis were obtained with an Autograph AG-5000A machine (Shimadzu, Kyoto, Japan). The microtomed surfaces of the unstretched sheets and stretched films were cut parallel to the stretching direction and observed by scanning electron microscopy (SEM; Hitachi Seisakusho, model S-510, Tokyo, Japan). Measurement of the R_a was carried out with a three-dimensional R_a meter (Kosaka Research Institute Co., model SE-3AK, Tokyo, Japan) with a stylus tip radius of 2 μm, a contact load of 30 mg, a stylus tip velocity of 0.1 mm/s, and a cutoff of 0.8 mm. The measurements were carried out through a length of 2.5 mm length, and a height of 500 points for each 2.5 μm was input by a data analyzer (Kosaka Research Institute Co., model TDA-21, Tokyo, Japan).

NUMERICAL ANALYSIS

For numerical analysis, we used finite element method (FEM) software by MARC (MSC Software Corp., Tokyo, Japan).

Model

The matrix polymer was considered a homogeneous, isotropic, elastic–plastic material.[18] Material constants were treated as isotropic and independent of strain rate. Geometrical nonlinearity was accounted for by Lagrangian remeshing. Each film was assumed to be a thin, two-dimensional body, and its deformation was treated as a plane strain problem.

Object of analysis

In the unstretched sheet, particles of incompatible polymers were randomly distributed throughout the matrix polymer. The numerical model we used is illustrated in Figure 1. In the FEM, the particle radius (r) was 5 μm. Further interaction between neighboring particles could be neglected.

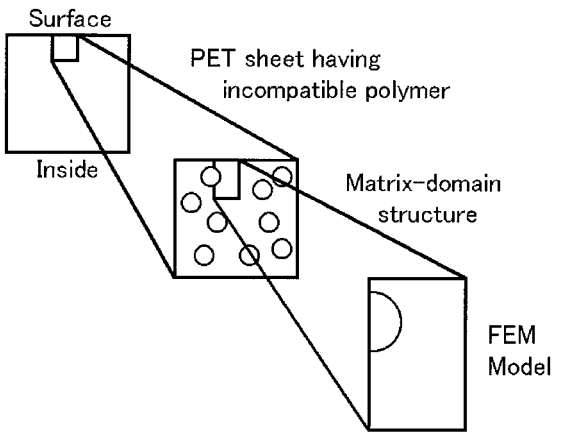

Figure 1 Relationship between the picture of the PET sheet with incompatible polymers and the finite element model.

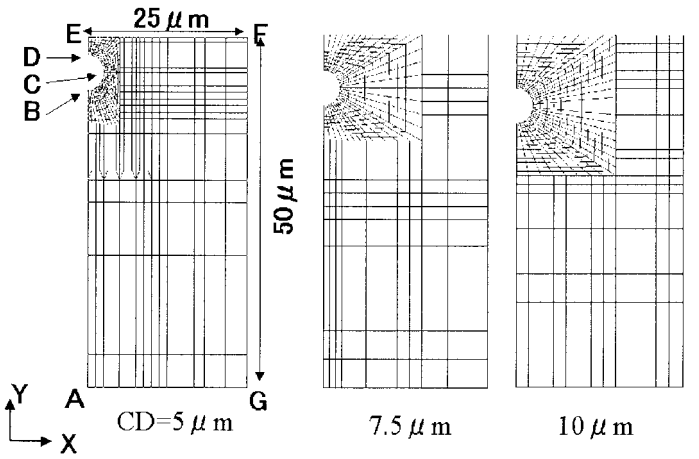

Figure 2 Finite element mesh.

Initial mesh and boundary conditions

Figure 2 shows the initial finite element mesh used to analyze the subsurface region of the film. In this study, three types of meshes were used with different intervals between the surface and the center of the particle: 5, 7.5, and 10 μm. As indicated, a half model was used, which accounted for symmetry, and quadrilateral generalized plane strain elements[13] were adopted. The semicircle at BCD in Figure 2 represents one half of a particle of the added incompatible polymer, and the mesh area is the PET phase. The fixed lines AE and AG define the x and y directions, respectively. All of the points on the line EF were constrained to undergo equal displacements in the y direction so that changes of the length in the y direction (L_y) were permitted and the mesh boundary AEFGA would maintain its rectangular outline throughout the deformation.

Material behavior used in the numerical analysis

Table II shows the conditions for the numerical analysis. To characterize the material behavior for the numerical analysis of PET, curves of true stress against logarithmic strain were obtained with a tensile testing machine. The test specimens were 40 mm wide, and the distance between the end grips was 40 mm. The strain rate was 0.333 s^{-1}. Poisson's ratio (ν) for PET was assumed to be 0.36. The von Mises yield criterion was used to define the onset of yielding under multiaxial stress.

TABLE II
Conditions for Numerical Analysis

Property	Value
E (MPa)	58.8
ν	0.36
σ_y (MPa)	0.42

Model of delamination

To model the phenomenon of interfacial delamination, critical values were defined for the stresses acting on the interface in the normal (σ_n) and tangential directions (σ_t) at the point of delamination. The critical stress at interfacial delamination (σ_r) was expressed as the ratio of the critical stress (σ_x) to the yield stress of PET (σ_{PET}), where σ_x was given by either σ_n or σ_t. The relationship between σ_n and σ_t was defined by the following equation:

$$\sigma_t = \sigma_n 3^{-1/2} \tag{1}$$

σ_n and σ_t at the interface between the particle and the matrix were calculated by extrapolation from stresses in the element of Gaussian integration points near that point. When either the σ_n or σ_t at the interface was above the critical value, interfacial delamination was assumed to occur, and the fixed displacement condition was removed from this point.

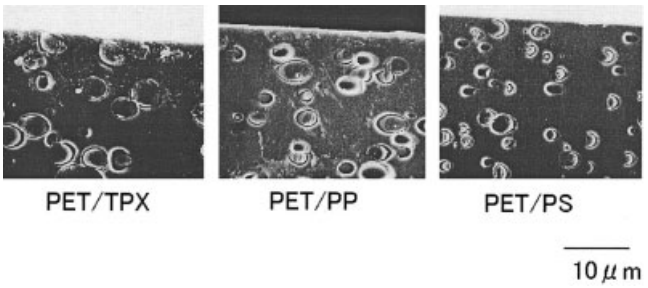

Figure 3 Photograph of casting sheets near the surface (cross-section).

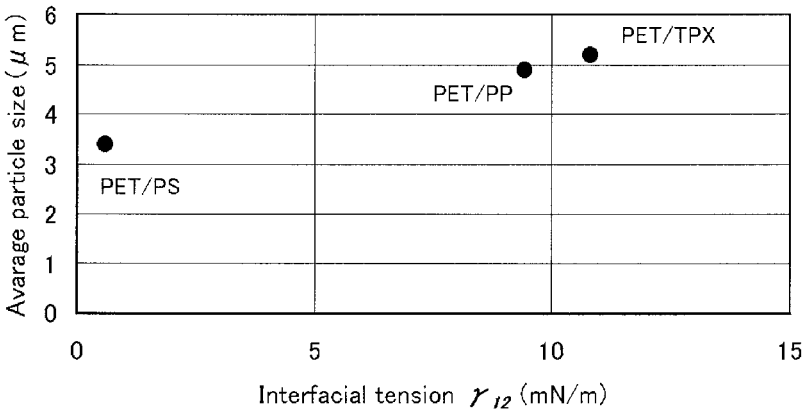

Figure 4 Relationship between the interfacial tension and the average particle size.

RESULTS AND DISCUSSION

Experimental results

Figure 3 shows the scanning electron micrographs of cross-sections for the unstretched PET films containing particles of TPX, PP, and PS, but the ratio of PET to incompatible polymer was 86:14 vol %. Figure 4 shows the relationship between the average particle size of the incompatible polymers and the interfacial tension between PET and the incompatible polymers. The weight-average particle diameter (d) was obtained by the following equation:

$$d = \sum n_i \times d_i^2 \Big/ \sum n_i \times d_i \qquad (2)$$

where d_i is the diameter of each particle and n_i is the number of particles in group i. The incompatible polymer particles were slightly drawn in the flow direction, so the particles were ellipsoid in shape. However, particle diameters were estimated from the area of the particle. As shown in Figure 4, the diameter of the particle of the incompatible polymers depended on the interfacial tension linearly. The electron micrographs also show that the particles were the same size, despite the position in the thickness direction.

Figure 5 shows the relationship between the volume of incompatible polymers and R_a. R_a was obtained by the following equation:

$$R_a = \frac{1}{L_x L_y} \int_0^{L_x} \int_0^{L_y} |f(x,y)| dx\, dy \qquad (3)$$

where L_x and L_y are the lengths through the x and y directions, respectively, and $f(x,y)$ is the relative height from the center line of the surface. For PET with no particles, the R_a difference between the unstretched sheet and the stretched film was small. However, for all of the PET films with particles, R_a of the stretched films was larger than the unstretched one. Furthermore, R_a increased with increasing amounts of incompatible polymer and decreased with increasing interfacial tension. These results suggest that the movement of the incompatible polymer particles to the surface region in the stretching process made the surface rougher.

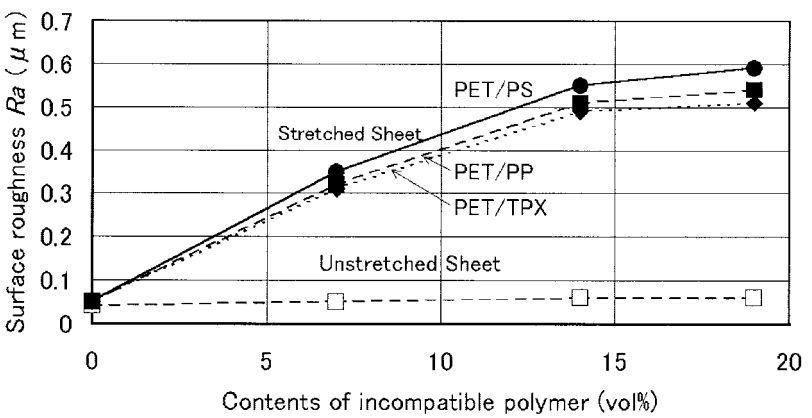

Figure 5 Relationship between the contents of incompatible polymers and R_a values.

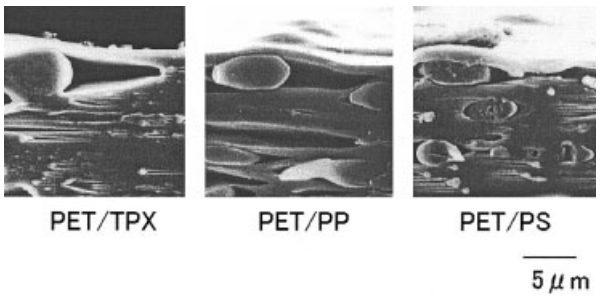

Figure 6 Photographs of stretched films near the surface (cross-section).

Figure 6 shows scanning electron micrographs of cross-section of the subsurface region of the stretched PET films containing particles of TPX, PP, and PS. These micrographs show that the void and protrusion were generated around the incompatible polymer particles by stretching. With more detailed observation, a concavity around the protrusion was found.

Figure 7 shows the relationship between the ratio of the height of protrusion (h_1) to the diameter of an incompatible polymer particle and the interfacial tension. The figure suggests that the height of protrusion increased with decreasing interfacial tension.

Figure 8 shows the relationship between the aspect ratio of the voids and the interfacial tension, where the aspect ratio was the ratio of the length of the void to the diameter of the incompatible polymers. It was confirmed that an increase in the interfacial tension was associated with the aspect ratio of the void.

Numerical analysis by FEM

Representative deformation diagrams at uniaxial tensile strains (ε_n's) of 1.0 and 2.0 for σ_r's of 2.0 and 60.0 are shown in Figures 9 and 10. The results of the numerical analysis revealed that interfacial delamination did not occur when the critical stress was larger than 60.0, but the delamination easily occurred at lower critical stresses (<20.0). Also, the relationship between σ_r and the aspect ratio of the void is shown in Figure 11. The aspect ratio of the void was the largest when σ_r was 1.2 and decreased with increasing σ_r.

Figure 12 shows the relationship between σ_r and the ratio of protrusion height (h_2) to particle diameter. When σ_r was 60.0, h_2 was the largest, and this value increased with decreasing interfacial delamination stress. By detailed tracing of a delamination diagram for ε_n = 1.0 and σ_r = 2.0 in Figure 9, we observed a concavity around the protrusion. This refers to the observation of a cross-section for PET–PP by SEM, as shown in Figure 6. This concavity appeared only in the early stage of delamination; it was extinguished at ε_n = 2.0. Detailed numerical analysis suggested that this concavity occurred by the compression stress to the y direction, and it was extinguished when ε_n = 2.0 by a decrease in the compressive stress in later stages.

Figure 13 shows representative diagrams of the changing of the depth of the particle from the surface at an extension ratio of ε_n = 2.0 for σ_r = 2.0 by a changing in the distance from the surface to the center of the particle. Our intuition suggested that the lower the depth was, the higher the height protrusion was. The experimental results could not be confirmed, but numerical analysis easily confirmed our intuition. Figure 14 shows the relationship between the height of protrusion and the depth of the particle. This suggests that the depth increased with decreasing height of protrusion.

Comparison between the numerical analysis and the experimental results

In a previous study,[16,17] the authors concluded that interfacial properties are important for controlling void generation because the aspect ratio of the void in the bulk increases with increasing interfacial tension between PET and incompatible polymers.

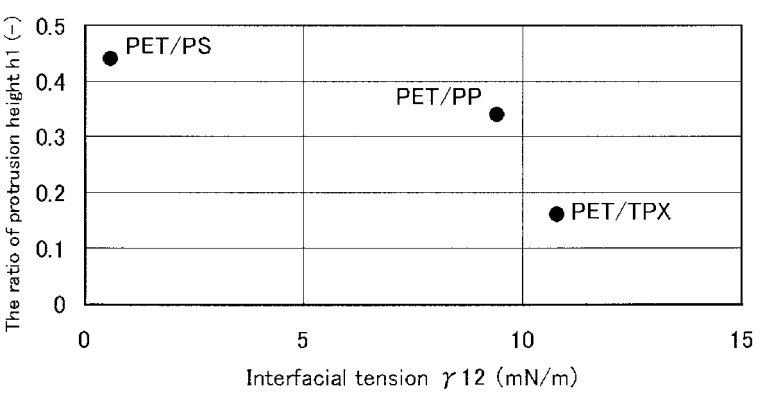

Figure 7 Relationship between the interfacial tension and h_1.

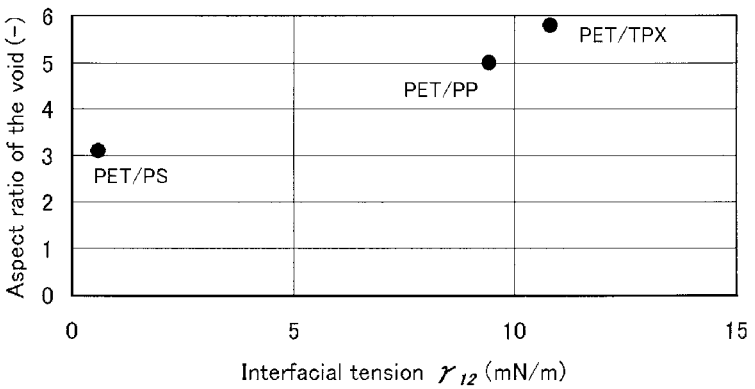

Figure 8 Relationship between the interfacial tension and the aspect ratio of the void.

In this study, we confirmed that the void generation in the subsurface region had the same behavior in the bulk region. Also supported was the fact that the interfacial tension in the experiment reflected the interfacial critical stress in the numerical analysis.

Further, it was significant that the movement up of an incompatible polymer particle to the surface by stretching generated protrusion. This phenomenon depended on the interfacial properties between PET and the incompatible polymer particles as well as void generation. In fact, the height of protrusion increased with decreasing interfacial tension experimentally and with increasing interfacial delamination stress numerically. This fact is important to suggest that increasing the void size generated a reduction in the height of protrusion when one considers the relationship between the void generation and the interfacial properties.

As shown by detailed analysis of the numerical results, each extended state in parts of PET matrix depended on the generating protrusion in addition to the qualitative coincidence of the experimental and numerical results. When the interfacial delamination occurred between the matrix and the particle, the PET matrix near point D–E in Figure 9 was largely extended in the x direction and largely compressed in the y direction despite the normal matrix extension in the x direction and compression in the y direction near point C′ because the void was generated. As a result, the height of protrusion was low because the difference in these deformed states was small. In contrast, when interfacial delamination did not occur, the PET matrix around point C in Figure 10 was largely in the y direction and compressed a little in the x direction. However, the PET matrix between the surface and the particle (near point D–E in Fig. 10) was extended less in the y direction and was less compressed in the x direction. Consequently, the difference between these deformed states formed the protrusion.

More interesting results confirmed that we needed to consider the effect of a concavity and a protrusion to understand R_a of the void-containing films. A slight concavity was observed in both the experiment (PET/PP in Fig. 6) and the numerical analysis (Fig. 9). As shown by detailed observation of the deformed diagram, the larger compression of the PET matrix between the surface and the void (near point H in Fig. 9) than the other positions in the matrix caused the concavity. The protrusion was distinguishable in the last stage of stretching because the whole PET matrix was homogeneously deformed in the numerical analysis. Experimentally, the protrusion was sometimes observed because it was supposed to relate to an orientation of the PET molecule or the neighborhood of other particles.

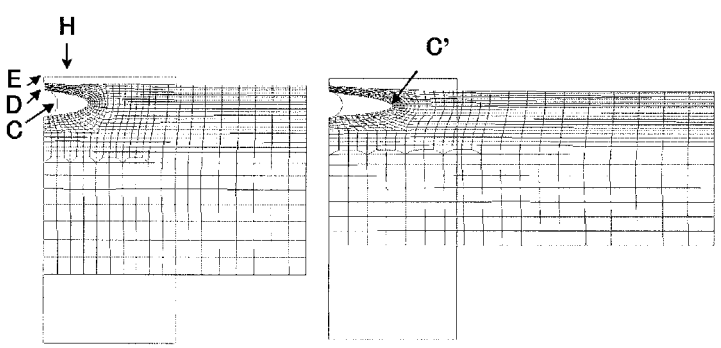

Figure 9 Deformation diagrams for the analysis of the region near the surface at σ_r = 2.0 [ε_n = (left) 1.0 and (right) 2.0].

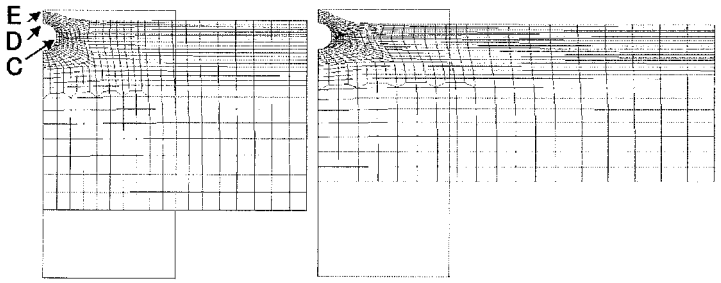

Figure 10 Deformation diagrams for the analysis of the region near the surface at $\sigma_r = 60.0$ [ε_n = (left) 1.0 and (right) 2.0].

In this study, the mechanism of void and protrusion generation could be assumed with a two-dimensional model embedded a rigid particle. For precise analysis, we plan to study this quantitatively. An example is calculation of stress distribution around a particle by stretching. Liu and Nauman calculated stress distribution within a spherical particle and in an otherwise uniform matrix with spherical harmonic function.[20] According to this calculation, the maximum was the stress parallel to the addition of tension at the pole and the stress perpendicular to the addition of tension at the equator of a particle. This model was only calculated without stretching; however, it will apply to cases with a large deformation.

Discussion

Surface topography

For each pair considered in this study, the interfacial tension could be expressed with the following equation[21]

$$\gamma_{12} = \frac{(RTB)^{1/2}}{2} \sum \beta_{ij} \left[1 + \frac{(\beta_A - \beta_B)^2}{3(\Sigma \beta_{ij})^2} \right] \qquad (4)$$

where $B = (\delta_i - \delta_j)^2$ is the interaction energy, a function of the solubility parameter (δ); $\beta_A^2 = (1/6)\rho_A b_A^2$, where ρ_A is the density and b_A is the statistical segment length of PET; $\beta_B^2 = (1/6)\rho_B b_B^2$, where ρ_B is the density, and b_B is the statistical segment length of incompatible polymer; β_{ij} is a dimensional constant; T is the blend temperature; and R is the gas constant. Thus, a decrease in B through the minimization of the difference in δ_{ij} reduced γ_{12} and promoted compatibility between the PET–polymer particle phases. The δ_{ij} data for the blends considered in this study did conform to this criterion as shown in Table III, where the δ values were calculated according to the method of Hoftyzer and Van Krevelen[22] on the basis of group contributions.

A reduced γ_{12} increased adhesion between the phases:

$$W = \gamma_1 + \gamma_1 - \gamma_{12} \qquad (5)$$

where W is the thermodynamic work of adhesion (J/m^2). Enhanced adhesion at the interface (a lower γ_{12}) contributed to greater mechanical stress transfer to the particle surface during the drawing of the PET film with the concomitant higher protrusion. The delamination stress was indeed given by[23]

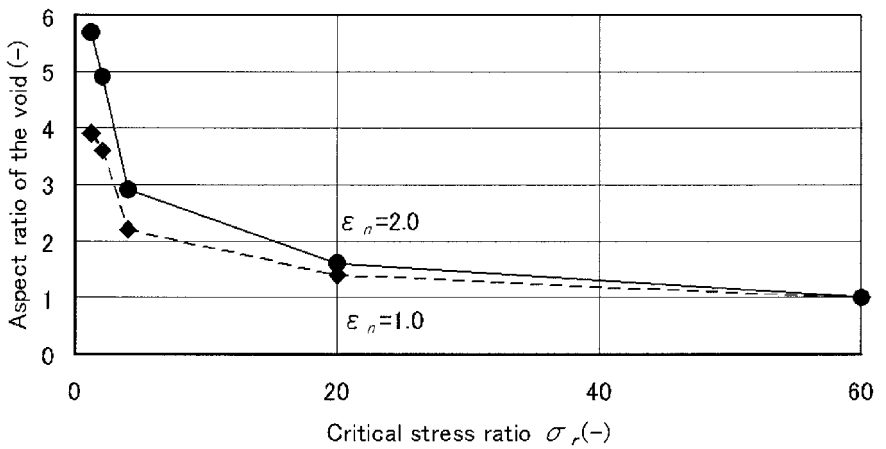

Figure 11 Relationship between σ_r and the aspect ratio of the void.

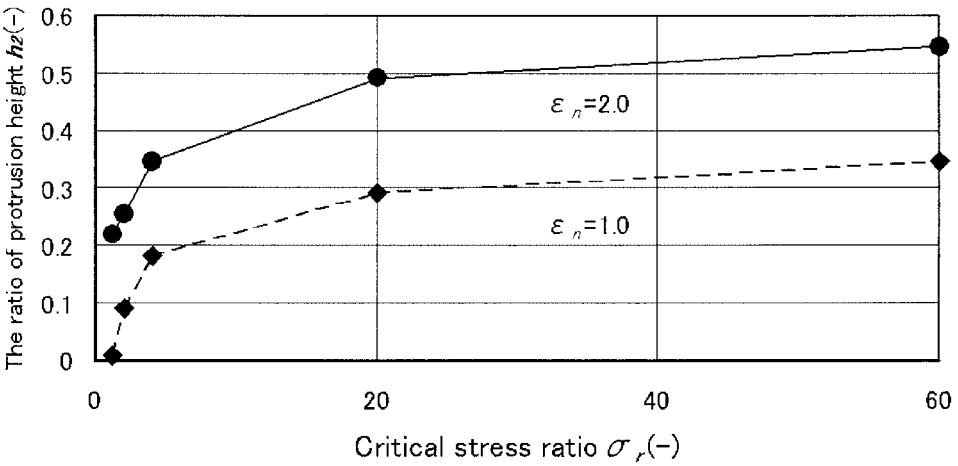

Figure 12 Relationship between σ_r and h_2.

$$\sigma = (4\pi GE/3r)^{1/2} \quad (6)$$

where σ is the delamination stress (Pa), G is the debond fracture energy or measured adhesion (J/m^2), E is the PET elastic modulus (Pa), and r is the particle radius (m). According to this equation, σ (and, hence, particle protrusion) is augmented by a higher G (a lower γ_{12}) but a smaller r, which is in good agreement with the data presented in Figure 7 when viewed in conjunction with Figure 4.

Void formation

The formation of vacuoles and the release of the PET matrix from the particle occurred at a critical stress, which was close to E. Theoretical calculations (supported by birefringence studies) of the stress pattern around a spherical particle have indicated that the points of maximum axial stress (in the direction of draw) should occur a short distance from the particle surface.[24] The lateral stress (y direction in the paper) was indeed found to be compressive. The calculation of lateral strain was far less than the axial strain and dropped even further at the weaker interface because of the earlier detachment of the particle from the PET matrix. This increased disparity in the axial and lateral strains for the weaker interface (PET/PP and PET/TPX) explained in part the observed concavity.

Model

The critical stress for matrix cavitation near a spherical inclusion was given by[23]

$$\sigma_c = 5E/12 \quad (7)$$

where σ_c is the critical rupture stress and E is the elastic modulus of PET. It translated to a value of σ_r close to 60 for E = 58.8 MPa and a yield stress (σ_y) of 0.42 MPa. The value was agreement with the calculation that delamination did not occur at σ_r = 60.0.

Viscoelasticity [$E = f(t)$], draw ratio, and temperature should be included in the list of parameters used to investigate the effects of strain rate, the extent of strain deformation, and the viscosity on surface topography in future studies.

CONCLUSIONS

This study confirmed that stretching generates voids and protrusions in PET films containing incompatible polymer particles. The following conclusions were reached on the basis of experimental testing and numerical analysis, in which an FEM model was applied to the films, which were assumed to exhibit elastic–plastic behavior:

1. Interfacial properties are important to void generation in subsurface region and in the bulk.
2. Protrusion formation is caused by movement up a polymer particle and depends on interfacial properties and void generation.
3. Concavity is also necessary to understand the surface structure of film along with protrusion.

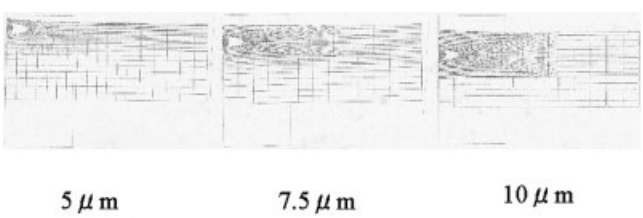

Figure 13 Representative deformation diagrams for the analysis of the region near surface at σ_r = 2.0 changing distance from the surface to the center of the particle.

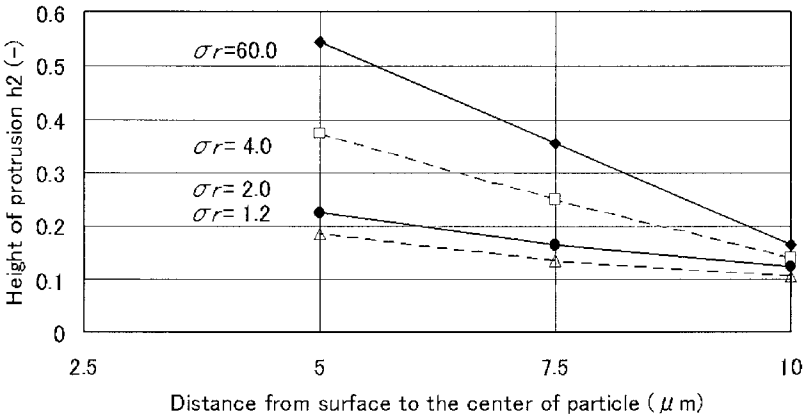

Figure 14 Relationship between distance from the surface to the center of the particle and h_2 numerically.

4. The position across the thickness of the particle should affect the height of protrusion.
5. In general, the character of the interface may influence the surface topography of the drawn film. An increase in the interfacial adhesion aided stress transfer between the phases in the particle-doped PET film with the attendant higher R_a. In this study, this was achieved by a decrease in the interfacial tension. However, other promising methods, such as the use of a reactive compatibilizer, may also augment adhesion and, thus, offer exiting opportunities to influence the surface topography of the film.
6. Delamination and cavitation during draw should result in the volume dilation of the film. Gas dilatometry may be used to obtain better insight into the process of void formation during the stretching of the film.

The authors thank Mr. Takaya Kobayashi of Mechanical Design and Analysis for advice on numerical analysis and Toyobo Co., Ltd., for permission to publish this work.

TABLE III
δ and B Values for PET, TPX, PP, and PS

Material	δ_1 (MPa)$^{1/2}$	δ_2 (MPa)$^{1/2}$	B (MPa)
PET/TPX	21.0	14.4	43.6
PET/PP	21.0	15.6	29.2
PET/PS	21.0	18.0	9.0

References

1. Abe, K. Kogyo Zairyo 1993, 41, 25.
2. Ouchi, I. Trans Mater Res Soc Jpn B 1993, 15, 901.
3. Uchida, E.; Iwata, H.; Ikada, Y. Polymer 2000, 41, 3609.
4. Wantai, Y.; Bengt, R. J Appl Polym Sci 1996, 62, 533.
5. Seto, F.; Kishida, A.; Muraoka, Y.; Akashi, M. J Appl Polym Sci 1999, 74, 1524.
6. Deng, C. S.; Assender, H. E.; Dinelli, F.; Kolosov, O. V.; Briggs, A. D.; Miyamoto, T.; Tsukahara, Y. J Polym Sci Part B: Polym Phys 2000, 38, 3151.
7. Jahromi, S.; Moosheimer, U. Macromolecules 2000, 33, 7582.
8. Inagaki, N.; Tasaka, S.; Shimada, S. J Appl Polym Sci 2000, 79, 808.
9. Dinelli, F.; Assender, H. E.; Kirov, K.; Kolosov, O. V. Polymer 2000, 41, 4285.
10. Tokuda, K. Abst. Pap.; First Ann. Meeting Japan Society for Polym Process, Tokyo, Japan, June 27–28, 1990, p 235.
11. Gould, S. A. C.; Schiraldi, D. A.; Occelli, M. L. CHEMTECH 1998, 28, 35.
12. Johnson, R. W.; Abrams, L.; Maynard, R. B.; Amick, T. J. Coat Papermakers Conf 1998, 1, 337.
13. Kugo, K.; Watanabe, E.; Kitaura, T.; Nishino, J. Compos Interfaces 1995, 3, 221.
14. Khan, M. B.; Keener, C. Polym Eng Sci 1996, 36, 1290.
15. Shertukde, V. V.; Kale, D. D. J Polym Mater 1999,16, 55.
16. Ito, K.; Nonomura, C.; Suzuki, T.; Ishihara, H. J Soc Mater Sci Jpn (Zairyou) 2000, 49, 1270.
17. Ito, K.; Nonomura, C.; Suzuki, T.; Ishihara, H.; Yamada, T. J Jpn Soc Polym Proc (Seikeikako) 2001, 13, 408.
18. Yamada, Y. Sosei Nendansei; Baifukan: Tokyo, 1990.
19. Wu, S. In Polymer Handbook, 4th ed.; Brandrup, J.; Immergut, E. H.; Grulke, E. A., Eds.; Wiley: New York, 1999; Vol. 4, p IV–521.
20. Liu, S. H.; Nauman, E. B. J Mater Sci 1990, 25, 2071.
21. Helfand, E.; Sapse, A. M. J Chem Phys 1975, 62, 1327.
22. Van Krevelen, D. W. Properties of Polymers, 3rd ed.; Elsevier: Amsterdam, 1997.
23. Gent, A. N. J Mater Sci 1980, 15, 2884.
24. Sezawa, K.; Miyazaki, B. J Soc Mech Eng 1928, 31, 625.